Propagation effects of isolated attosecond pulse generation with a multicycle chirped and chirped-free two-color field

Hongchuan Du and Bitao Hu*
School of Nuclear Science and Technology, Lanzhou University, Lanzhou 730000, China
(Received 16 May 2011; published 12 August 2011)

We present a theoretical study of isolated attosecond pulse generation with a multicycle chirped and chirped-free two-color field. We show that the bandwidth of the extreme ultraviolet supercontinuum can be extended by combining a multicycle chirped pulse and a multicycle chirped-free pulse. Also, the broadband supercontinuum can still be generated when the macroscopic effects are included. Furthermore, the macroscopic effects can ameliorate the temporal characteristic of the broadband supercontinuum of the single atom, and eliminate the modulations of the broadband supercontinuum. Thus a very smooth broadband supercontinuum and a pure isolated 102-as pulse can be directly obtained. Moreover, the structure of the broadband supercontinuum can be steadily maintained for a relative long distance after a certain distance.

DOI: 10.1103/PhysRevA.84.023817 PACS number(s): 42.65.Ky, 32.80.Rm, 42.65.Re

I. INTRODUCTION

In the past decade, remarkable advances have been achieved in the field of ultrafast optics [1]. Particularly, the generation of attosecond pulses has opened the door to the same dramatic applications to the study of ultrafast processes with extremely short time scales, such as the electronic dynamics inside atom [2] and on the surface of metal nanostructure [3]. There is no doubt that the future of attosecond physics as well as attosecond science will critically rely on the development of technologies for generating single attosecond pulses with both high intensity and short duration. Nowadays, isolated attosecond pulses have been experimentally generated mainly using two techniques: a few-cycle driving pulse [4–6] or polarization gating [6–9]. Very recently, the 100-as barrier has been first brought through by Goulielmarkis *et al*. [4] using the first approach. In their experiment, a sub-4-fs near-single-cycle driving pulse has been employed to generate a 40-eV supercontinuum and an 80-as pulse with the pulse energy of 0.5 pJ has been filtered out. Unfortunately, only very few laboratories can routinely produce such short driving pulses, which limits the spreading of attosecond sources. The polarization gating is based on the strong dependence of the high-harmonic generation (HHG) on the ellipticity of the driving pulse and relaxes the required pump pulse duration for creating an isolated attosecond pulse. Recently, a very broadband xuv continuous spectrum, which supports 16-as isolated pulse generation, has been produced with a double-optical-gating technique [10]. Using the few-cycle laser-pulse polarization gating technique, Sansone *et al*. [6] have obtained a single 130-as pulse generated from a 36-eV continuum after compensating for the harmonic chirp. This technique still requires the state-of-the-art 5–7 fs pump pulses with carrier-envelope phase stabilized and can't generate intense isolated attosecond pulses.

The mechanism of HHG can be well understood using the three-step model: [11] ionization, acceleration, and recombination. During the recombination, a photon is emitted with energy equal to the ionization potential plus the kinetic energy of a recombining electron. This classical picture suggests that the HHG process can be manipulated via modulating the external field or the target to broaden the bandwidth or enhance the efficiency of high-harmonic spectrum. Besides the above-mentioned two techniques (a few-cycle driving pulse or polarization gating), the two-color and multicolor schemes have also been introduced to control electron dynamics or confine the ionization process within a short time to generate broadband isolated attosecond pulses [12–21]. Especially, the multicycle two-color field is one of the most promising and extensively used methods to generate a routinely isolated attosecond pulse in ordinary laboratories. The chirped femtosecond pulse is another promising technique for performing quantum control of the HHG process [22–25]. By chirping a few-cycle laser pulse, Carrera *et al*. extended dramatically the high-harmonic cutoff and generated an isolated attosecond pulse with the duration of 108 as, theoretically [24]. However, it should be stressed that this scheme has been considered only for a single atom. Since ionization is concomitant with the HHG, and the ionized gas medium will lead to a distortion and phase shift of the laser pulse after propagation [26], macroscopic effects may significantly alter the single-atom results [27]. This is a very serious issue for the HHG. Altucci *et al*. investigated macroscopic effects of attosecond pulse generation in a few-cycle [28] and multicycle [29–31] polarization gating regime. Schiessl *et al*. investigated the high-order harmonic generation with the two-color field considering the influence of propagation effects [32]. However, to the best of our knowledge, the propagation effects of isolated attosecond pulse generation with the multicycle chirped and chirped-free two-color field have never been reported.

In this paper, we aim at providing a method of isolated attosecond pulse generation combining a multicycle chirped and chirped-free two-color field with a three-dimensional propagation model. Compared with the case of using a multicycle chirped-free two-color field, both the harmonic cutoff and the bandwidth of the extreme ultraviolet supercontinuum can be extended by combining a multicycle chirped pulse and a multicycle chirped-free pulse. Furthermore, the broadband supercontinuum can still be obtainable when the macroscopic

*hubt@lzu.edu.cn

effects are included. The macroscopic effects can ameliorate the temporal characteristic of the broadband supercontinuum of the single atom, and eliminate the modulations of the broadband supercontinuum. Thus a very smooth broadband supercontinuum and a pure isolated 102-pulse can be directly obtained. Moreover, the structure of the broadband supercontinuum can be steadily maintained for a relatively long distance after a certain distance.

II. THEORETICAL METHODS

In our calculation, the Lewenstein model [33] is applied to qualitatively give a harmonic spectrum in the two-color field. In this model, the instantaneous dipole moment of an atom is described as (in atom units)

$$d_{\rm nl} = i\int_{-\infty}^{t} dt' \left(\frac{\pi}{\varepsilon + i(t-t')/2}\right)^{3/2} \times d^*[p_{\rm st}(t',t) - A(t)]d[p_{\rm st}(t',t) - A(t')] \times \exp[-iS_{\rm st}(t',t)]E_f(t')g(t') + \text{c.c.} \quad (1)$$

In this equation, $E_f(t)$ is the electric field of the laser pulse, $A(t)$ is its associated vector potential, and ε is a positive regularization constant. $p_{\rm st}$ and $S_{\rm st}$ are the stationary momentum and quasiclassical action, which are given by

$$p_{\rm st}(t',t) = \frac{1}{t-t'}\int_{t'}^{t} A(t'')dt'', \quad (2)$$

$$S_{\rm st}(t',t) = (t-t')I_p - \frac{1}{2}p_{\rm st}^2(t',t)(t-t') + \frac{1}{2}\int_{t'}^{t} A^2(t'')dt'', \quad (3)$$

where I_p is the ionization energy of the atom and $d(p)$ is the dipole matrix element for transitions from the ground state to the continuum state. For hydrogen-like atoms, it can be approximated as

$$d(p) = i\frac{2^{7/2}}{\pi}(2I_p)^{5/4}\frac{p}{(p^2+2I_p)^3}. \quad (4)$$

The $g(t')$ in Eq. (1) represents the ground-state amplitude:

$$g(t') = \exp\left(-\int_{-\infty}^{t}\omega(t'')dt''\right), \quad (5)$$

where $\omega(t'')$ is the ionization rate, which is calculated by the Ammosov-Delone-Krainov (ADK) tunneling model [34]:

$$\omega(t) = \omega_p|C_{n^*}|^2\left(\frac{4\omega_p}{\omega_t}\right)^{2n^*-1}\exp\left(-\frac{4\omega_p}{3\omega_t}\right), \quad (6)$$

where

$$\omega_p = \frac{I_p}{\hbar}, \quad \omega_t = \frac{e|E_f(t)|}{\sqrt{2m_eI_p}}, \quad n^* = Z\left(\frac{I_{\rm ph}}{I_p}\right)^{1/2}, \quad |C_{n^*}|^2 = \frac{2^{2n^*}}{n^*\Gamma(n^*+1)\Gamma(n^*)}, \quad (7)$$

where Z is the net resulting charge of the atom, $I_{\rm ph}$ is the ionization potential of the hydrogen atom, and e and m_e are electron charge and mass, respectively.

The harmonic spectrum is then obtained by Fourier transforming the time-dependent dipole acceleration $\vec{a}(t)$:

$$a_q(\omega) = \left|\frac{1}{T}\int_0^T \vec{a}(t)e^{-iq\omega t}dt\right|^2, \quad (8)$$

where $\vec{a}(t) = \ddot{\vec{d}}_{nl}(t)$ and T and ω are the duration and frequency of the driving pulse, respectively. q corresponds to the harmonic order.

The collective response of the macroscope medium is described by the propagation of the laser and the high-harmonic field, which can be written separately [35],

$$\nabla^2 E_f(\rho,z,t) - \frac{1}{c^2}\frac{\partial^2 E_f(\rho,z,t)}{\partial t^2} = \frac{\omega_p^2(\rho,z,t)}{c^2}E_f(\rho,z,t), \quad (9)$$

$$\nabla^2 E_h(\rho,z,t) - \frac{1}{c^2}\frac{\partial^2 E_h(\rho,z,t)}{\partial t^2} = \frac{\omega_p^2(\rho,z,t)}{c^2}E_h(\rho,z,t) + \mu_0\frac{\partial^2 P_{nl}(\rho,z,t)}{\partial t^2}, \quad (10)$$

where E_f and E_h are the laser and high-harmonic field; ω_p is the plasma frequency and is given by $\omega_p = e\sqrt{n_e(\rho,z,t)/m_e\epsilon_0}$ and $P_{\rm nl} = [n_0 - n_e(\rho,z,t)]d_{\rm nl}(\rho,z,t)$ is the nonlinear polarization generated by the medium. n_0 is the gas density and $n_e = n_0\{1 - \exp[-\int_{-\infty}^{t} w(t')]dt'\}$ is the free-electron density in the gas. This propagation model takes into account both the temporal plasma-induced phase modulation and the spatial plasma lensing effects, but does not consider the linear gas dispersion, the depletion of the fundamental beam during the HHG process, and absorption of high harmonics, which is due to the low gas density [35]. Then the induced refractive index n can be approximately described by the refractive index in vacuum ($n = 1$). These equations can be solved with the Crank-Nicholson method. The calculation details can be found in [35–37].

III. RESULTS AND DISCUSSION

In order to clearly demonstrate our scheme, we first investigate the HHG process according to the classical three-step model [11]. In our scheme, the electric field is given by

$$E(t) = E_0 f_0(t)\cos[\omega_0 t + \delta(t)] + E_1 f_1(t)\cos(\omega_1 t + \phi_{\rm CEP}), \quad (11)$$

where E_0 and E_1 are the amplitudes and ω_0 and ω_1 are the frequencies of the driving and controlling fields, respectively; $\phi_{\rm CEP}$ is the relative phase and is set as -0.15π; $f_0(t) = \exp[-2\ln(2)t^2/\tau_0^2]$ and $f_1(t) = \exp[-2\ln(2)t^2/\tau_1^2]$ present the pulse envelopes of the driving and controlling fields. τ_0 and τ_1 are the pulse durations (full width at half maximum). For the chirped case, the time-varying carrier-envelope phase (CEP) of the driving pulse is given by $\delta(t) = -\beta\tanh(t/\tau)$. β and τ are set as 6.25 and 800 a.u., respectively. For the chirped-free case, the time-varying CEP of the driving pulse is given by $\delta(t) = 0$. In our simulation, we choose $\omega_0 = 0.057$ a.u. and $\omega_1 = 0.0285$ a.u. corresponding to $\lambda_0 = 800$ nm and $\lambda_1 = 1600$ nm, respectively. E_0 and E_1 are set as 0.1 a.u. and $\sqrt{0.1}E_0$, respectively. $\tau_0 = 3T_0$ and $\tau_1 = 2T_1$, where T_0 and T_1 are the periods of the driving and controlling fields. Since the

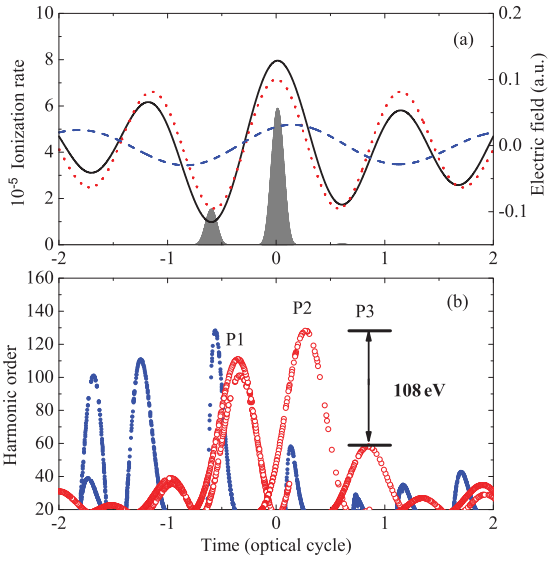

FIG. 1. (Color online) (a) Electric fields of the chirped driving pulse (red dotted curve), the controlling pulse (blue dashed curve), the chirped two-color field (solid black curve), and the ADK ionization rate in the chirped two-color field (filled gray curve). (b) Classical sketch of the electron dynamics in the chirped two-color pulse.

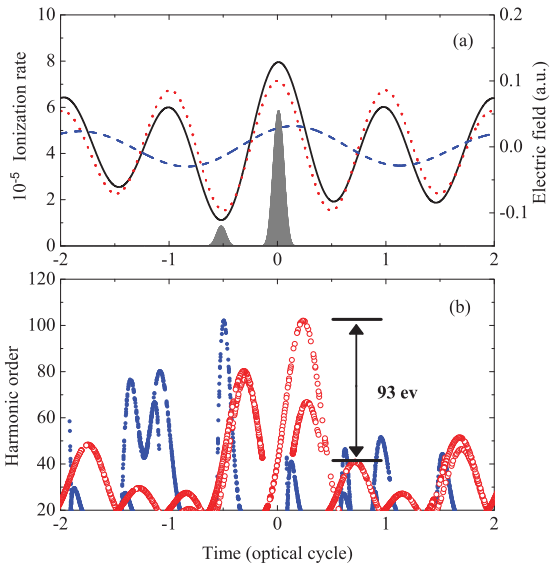

FIG. 2. (Color online) (a) Electric fields of the chirped-free driving pulse (red dotted curve), the controlling pulse (blue dashed curve), the chirped-free two-color field (solid black curve), and the ADK ionization rate in the chirped-free two-color field (filled gray curve). (b) Classical sketch of the electron dynamics in the chirped-free two-color pulse.

laser intensity is far below the saturation intensity of the target atom (here the helium atom is chosen), the HHG process can be well depicted in terms of the classical electron trajectories and the ADK ionization rate [34]. Figure 1 shows the classical picture of the HHG process in the multicycle chirped two-color field. We show the ionization rate (gray filled curve) in the chirped two-color field and the electric fields of the chirped driving pulse (red dotted curve), controlling pulse (blue dashed curve), and the chirped two-color field (solid black curve) in Fig. 1(a). Figure 1(b) shows the electron trajectories in the chirped two-color field. The ionization and recombination times are shown in blue dots and red circles, respectively. As shown in this figure, there are three main peaks (marked P1, P2, and P3) with maximum harmonic order of 111, 128, and 58, respectively. One can clearly see that the returning probability of the electron path P1 is much lower than those of P2 and P3 owing to the lower ionization rate; thus the harmonic yield for P1 is much lower than others. Taking account of the above results, we can conclude that a supercontinuum between the maximum energies of P2 and P3 (with the bandwidth 108 eV) can be generated. For comparison, we also investigate the classical picture in the chirped-free two-color field, which is shown in Fig. 2. It is clear that a supercontinuum between the 41st and 101st harmonics with the bandwidth of 93 eV can be generated. So the bandwidth of the supercontinuum can be extended by using the chirped two-color field.

In the following, we further calculated the harmonic spectrum by using the Lewenstein model [33] to confirm the classical sketch above. Here the neutral species depletion is considered using the ADK ionization rate. The harmonic spectrum is shown in Fig. 3(a). The harmonic spectra of the chirped two-color field and the chirped-free two-color field are shown in bold black curve and thin red curve, respectively. As shown in this figure, for the chirped two-color field, the spectrum cutoff is approximately the 132nd harmonic (205 eV), and the spectrum above the 64th (99 eV) becomes continuous, which is in agreement with the classical approaches shown in Fig. 1. The modulations on the supercontinuum are due to the interference of the short and the long quantum paths. The spacing of the spectral modulation is about 5.3 eV. Moreover, the modulation rate changes as the harmonic order increases.

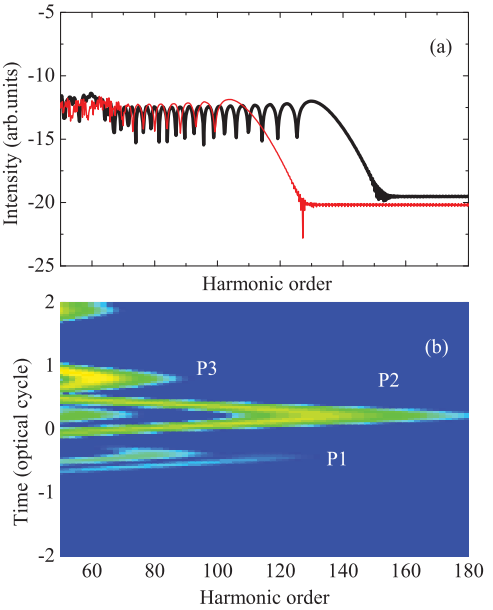

FIG. 3. (Color online) (a) Harmonic spectra in the chirped two-color pulse (bold black curve) and in the chirped-free two-color pulse (thin red curve) and (b) time-frequency distribution in the chirped two-color pulse.

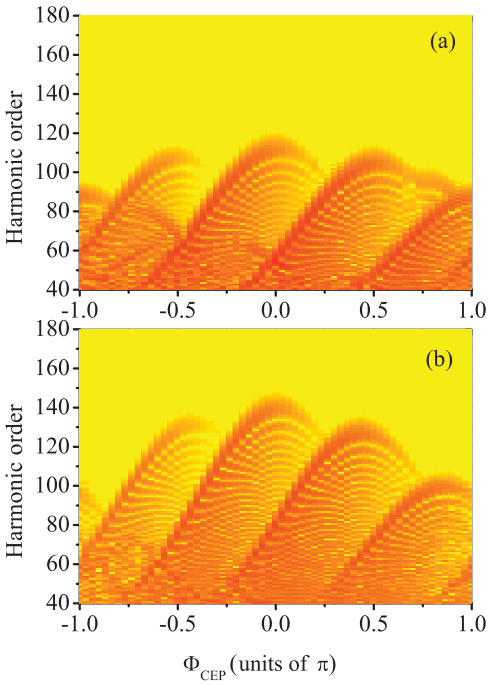

FIG. 4. (Color online) Harmonic spectrum as a function of ϕ_{CEP} (a) with the chirped-free two-color pulse and (b) with the chirped two-color pulse.

This is because the time spacing between the short and the long quantum paths decreases with the increasing harmonic order. For the chirped-free two-color field, the spectrum cutoff is approximately the 105th harmonic (163 eV) and the spectrum above the 70th is continuous. The bandwidth of the continuous is obviously smaller than the above classical results shown in Fig. 2, which results from the influences of other weaker quantum paths launched by a weaker part of the laser field. A deeper insight is obtained by investigating the emission times of the harmonics in terms of the time-frequency analysis method [38]. Figure 3(b) shows the time-frequency distribution of the HHG in the chirped two-color field. It can be seen that there are three main peaks contributing to the harmonics with the maximum orders of approximately the 113th, 132nd, and 64th, marked as P1, P2, and P3, respectively. The harmonic yields of the P1 are much lower than those of P2 and P3; thus the quantum path P2 contributes mainly to the harmonics above the 64th and forms a supercontinuum with bandwidth of 106 eV. These results are well in agreement with the classical results shown in Fig. 1. However, is the bandwidth of the supercontinuum in the chirped two-color field also larger than those of the supercontinuum in the chirped-free two-color field for other relative phase ϕ_{CEP}? To answer this question, we further investigate the harmonic spectra as a function of the relative phase ϕ_{CEP}. Figure 4 shows the continuous parts of the harmonic spectra generated (a) a chirped-free two-color field and (b) a chirped two-color field. As shown in this figure, the bandwidth of the supercontinuum in the chirped two-color field is larger than that of the supercontinuum in the chirped-free two-color field for all relative phase ϕ_{CEP}. In the following section, we will take $\phi_{CEP} = -0.15\pi$ and $\phi_{CEP} = 0.3\pi$ as examples to investigate the collective response of the harmonic spectra, respectively.

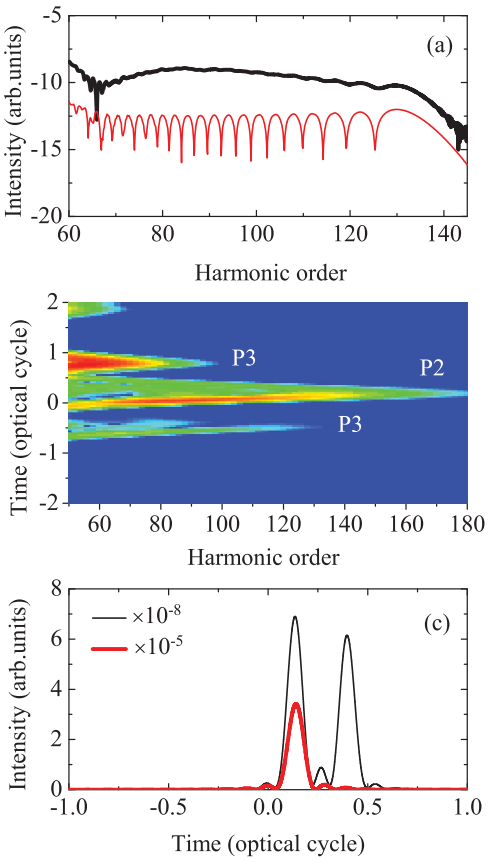

FIG. 5. (Color online) (a) On-axis (bold black curve) and single atom (thin red curve) high-order harmonic spectrum generated, (b) the time-frequency distribution of the macroscopic high-harmonic spectrum generated, and (c) the attosecond pulses generated by filtering the 100th–110th harmonics in the macroscopic high-harmonic spectrum (bold red curve) and in the single atom high-harmonic spectrum (thin black curve) with the chirped two-color pulse for $\phi_{CEP} = -0.15\pi$. The same parameters as in Fig. 1.

The coexistence of the short and long trajectories as shown in Fig. 3 prevents the isolated attosecond pulse generation. However, it is well known that the collective response of the macroscopic gas allows one to adjust the phase-matching condition to eliminate one quantum trajectory [39,40]. To generate an isolated attosecond pulse, we perform the nonadiabatic three-dimensional (3D) propagation simulations [35] for fundamental and harmonic field in the gas target. We consider a tightly focused Gaussian laser beam with a beam waist of 25 μm and a 1.0-mm-long gas jet with a density of 2.6×10^{18} cm^3. The gas jet is placed 2 mm after the laser focus. Other parameters are the same as in Fig. 1. Figure 5 shows the broadband supercontinuum on the axis for $\phi_{CEP} = -0.15\pi$ (bold black curve). For comparison, the single-atom result is also presented (thin red curve). One can see that the interference fringes are largely removed after propagation. Particularly, the harmonics above the 67th are phase matched well and become smooth, indicating the elimination of one trajectory. In order to demonstrate our result, we perform the time-frequency distribution of the broadband supercontinuum after propagation shown in Fig. 5(b). It is clear that the intensity of the short quantum path is very strong and that of the

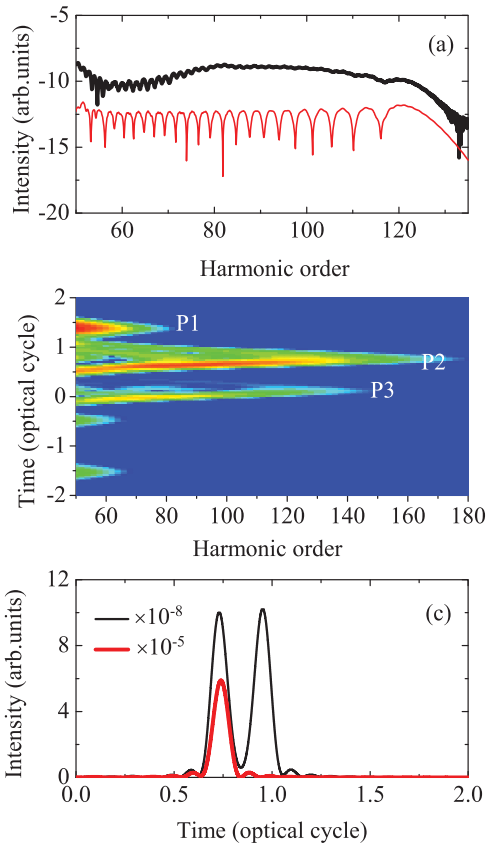

FIG. 6. (Color online) (a) On-axis (bold black curve) and single atom (thin red curve) high-order harmonic spectrum generated, (b) the time-frequency distribution of the macroscopic high-harmonic spectrum generated, and (c) the attosecond pulses generated by filtering the 100th–110th harmonics in the macroscopic high-harmonic spectrum (bold red curve) and in the single atom high-harmonic spectrum (thin black curve) with the chirped two-color pulse for $\phi_{\mathrm{CEP}} = 0.3\pi$. Other parameters as the same as in Fig. 1.

long quantum path is very weak. Therefore, the modulations induced by the interference between short and long quantum paths are too weak to be discernible. To unambiguously show that one of the trajectories has been eliminated, Fig. 5(c) shows that the attosecond pulses generated by filtering the 100th–110th harmonics on the macroscopic high-harmonic spectrum (bold red curve) and on the single atom high-harmonic spectrum (thin black curve). As shown in this figure, the long trajectory indeed is eliminated after propagation. For $\phi_{\mathrm{CEP}} = 0.3\pi$, the same conclusions can be obtained as shown in Fig. 6.

In this section, we investigate the attosecond pulse generation with the broadband supercontinuum on the axis after propagation. Figure 7(a) shows the temporal profile of the attosecond pulse by superposing the 75th–135th harmonics for $\phi_{\mathrm{CEP}} = -0.15\pi$. As shown in this figure, a pure isolated 102-as pulse can be directly obtained without any chirp compensation. Figure 7(b) shows the temporal profile of the attosecond pulse by superposing the 75th–125th harmonics for $\phi_{\mathrm{CEP}} = 0.3\pi$. As shown in this figure, a pure isolated 107-as pulse can be directly obtained without any chirp compensation. On the other hand, this supercontinuum with the bandwidth of

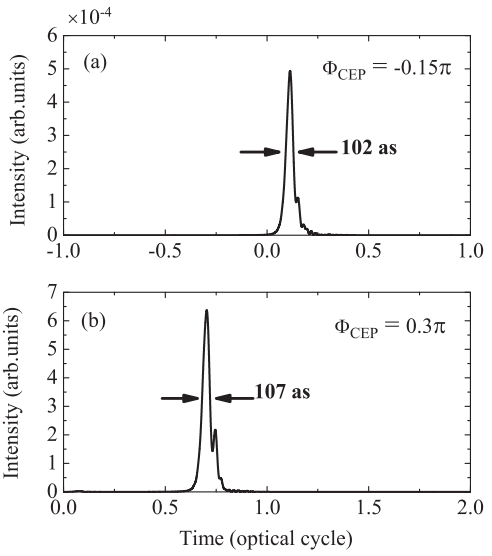

FIG. 7. Temporal profile of isolated attosecond pulses generated from the broadband supercontinuum on the axis after propagation (a) $\phi_{\mathrm{CEP}} = -0.15\pi$ and (b) $\phi_{\mathrm{CEP}} = 0.3\pi$.

over 100 eV can support an isolated 40-as pulse after proper chirp compensation.

The broadband supercontinuum is also influenced by the distance of propagation. Figure 8 shows the broadband supercontinua on the axis after propagating 0.75 mm, and 1.0 mm through the helium gas medium for $\phi_{\mathrm{CEP}} = -0.15\pi$ and $\phi_{\mathrm{CEP}} = 0.3\pi$, respectively. The entrance of the gas medium is located 2 mm downstream from the laser focus. Other parameters are the same as Fig. 1. For $\phi_{\mathrm{CEP}} = -0.15\pi$, as shown in Fig. 8(a), the phase-matching condition of the short quantum path is very satisfied for the harmonics above 67th, and a smooth broadband supercontinuum is obtained when the harmonics propagate 0.75 mm through the gas medium. When the distance of the propagation increases to 1.0 mm,

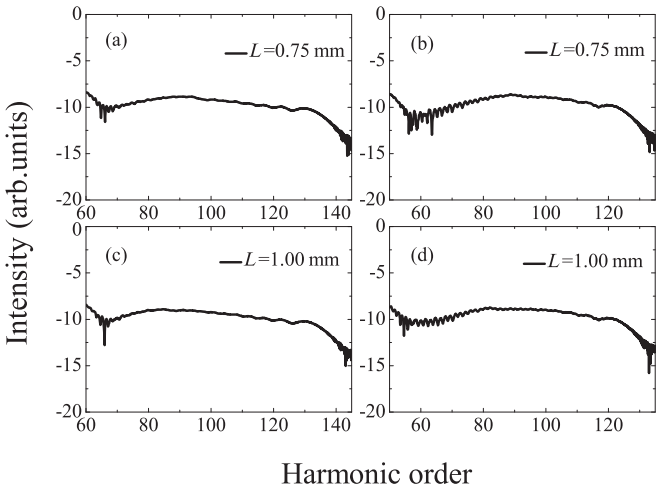

FIG. 8. Broadband supercontinuum after propagating (a) 0.75 mm for $\phi_{\mathrm{CEP}} = -0.15\pi$, (b) 0.75 mm for $\phi_{\mathrm{CEP}} = 0.3\pi$, (c) 1.0 mm for $\phi_{\mathrm{CEP}} = -0.15\pi$, and (c) 1.0 mm for $\phi_{\mathrm{CEP}} = 0.3\pi$. The entrance of the gas medium is located 2 mm downstream from the laser focus. Other parameters are the same as in Fig. 1.

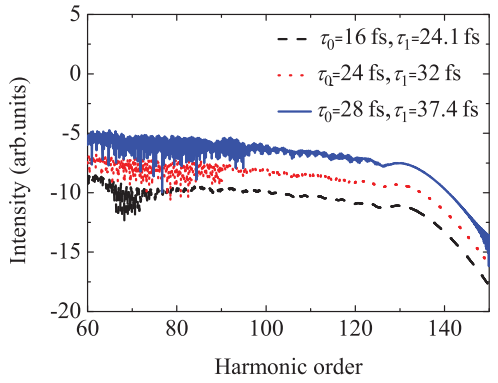

FIG. 9. (Color online) Harmonic spectra with different pulse durations. Other parameters are the same as in Fig. 3. The dotted red curve and solid blue curve have been shifted up 2.0 and 4.0 units, respectively.

the structure and intensity of the broadband supercontinuum hardly change. The same results can be obtained for $\phi_{\mathrm{CEP}} = 0.3\pi$. Thus the broadband supercontinuum is steady after propagating a distance between 0.75 and 1.00 mm, which makes the experiment more convenient.

We further investigated the influence of the pulse duration. The parameters are the same as in Fig. 5. Figure 9 presents on-axis high-order harmonic spectra after propagation with different pulse durations. For clarity, the harmonic spectra with the pulse duration $\tau_0 = 24$ fs, $\tau_1 = 32$ fs (dotted red curve) and $\tau_0 = 28$ fs, $\tau_1 = 37.4$ fs (solid blue curve) have been shifted up 2.0 and 4.0 units, respectively. One can see clearly that the smooth supercontinuum can be obtained up to $\tau_0 = 28$ fs, $\tau_1 = 37.4$ fs. However, the bandwidth of the supercontinuum decreases as the pulse duration increases. When the pulse duration is increased up to $\tau_0 = 64$ fs, $\tau_1 = 85$ fs, the bandwidth of the supercontinuum is decreased to about 30 eV and the ionization probability is below 1%.

IV. CONCLUSION

In summary, we investigate the macroscopic effects for quantum control of isolated attosecond pulse generation with the multicycle chirped two-color field. Compared to the case of using only a multicycle chirped-free two-color field, both the harmonic cutoff and modulated extreme ultraviolet supercontinuum can be extended by combining a multicycle chirped pulse with a multicycle chirped-free pulse. Furthermore, our numerical results also show that the broadband supercontinuum can still be obtainable when the macroscopic effects are included. Compared to the single-atom response, one quantum trajectory can be well selected after propagation. Thus a very smooth broadband supercontinuum and a pure isolated 102-as pulse can be directly obtained. Moreover, the structure of the broadband supercontinuum can be steadily maintained for a relative long distance after propagating a certain distance, which makes the experiment more convenient. Our quantum control scheme for the generation of the supercontinuum is also suitable for longer pulse duration. Although the bandwidth of the supercontinuum is decreased to about 30 eV, the upper limit for creating the isolated attosecond pulse can be increased up to $\tau_0 = 64$ fs, $\tau_1 = 85$ fs.

ACKNOWLEDGMENTS

This work was supported by National Natural Science Foundation of China (Grant Nos. 110775069, 91026021, 11075068, and 10875054) and the Fundamental Research Funds for the Central Universities (Grant No. lzujbky-2010-k08).

[1] F. Krausz and M. Ivanov, Rev. Mod. Phys. **81**, 163 (2009).
[2] R. Kienberger, E. Goulielmakis, M. Uiberacker, A. Baltuska, V. Yakovlev, F. Bammer, A. Scrinzi, Th. Westerwalbesloh, U. Kleineberg, U. Heinzmann, M. Drescher, and F. Krausz, Nature (London) **427**, 817 (2004).
[3] M. I. Stockman, M. F. Kling, U. Kleineberg, and F. Krausz, Nat. Photon. **1**, 539 (2007).
[4] E. Goulielmakis, M. Schultze, M. Hofstetter, V. S. Yakovlev, J. Gagnon, M. Uiberacker, A. L. Aquila, E. M. Gullikson, D. T. Attwood, R. Kienberger, F. Krausz, and U. Kleineberg, Science **320**, 1614 (2008).
[5] F. Ferrari, F. Calegari, M. Lucchini, C. Vozzi, S. Stagira, G. Sansone, and M. Nisoli, Nat. Photon. **4**, 875 (2010).
[6] G. Sansone, E. Benedetti, F. Calegari, C. Vozzi, L. Avaldi, R. Flammini, L. Poletto, P. Villoresi, C. Altucci, R. Velotta, S. Stagira, S. De Silvestri, and M. Nisoli, Science **314**, 443 (2006).
[7] P. Tzallas, E. Skantzakis, C. Kalpouzos, E. P. Benis, G. D. Tsakiris, and D. Charalambidis, Nat. Phys. **3**, 846 (2007).
[8] S. Gilbertson, S. D. Khan, Y. Wu, M. Chini, and Z. Chang, Phys. Rev. Lett. **105**, 093902 (2010).
[9] X. Feng, S. Gilbertson, H. Mashiko, H. Wang, S. D. Khan, M. Chini, Y. Wu, K. Zhao, and Z. Chang, Phys. Rev. Lett. **103**, 183901 (2009).
[10] H. Mashiko, S. Gilbertson, M. Chini, X. Feng, C. Yun, H. Wang, S. D. Khan, S. Chen, and Z. Chang, Opt. Lett. **34**, 3337 (2009).
[11] P. B. Corkum, Phys. Rev. Lett. **71**, 1994 (1993).
[12] E. J. Takahashi, P. Lan, O. D. Mücke, Y. Nabekawa, and K. Midorikawa, Phys. Rev. Lett. **104**, 233901 (2010).
[13] W. Cao, P. Lu, P. Lan, X. Wang, and G. Yang, Opt. Express **15**, 530 (2007).
[14] W. Hong, P. Lu, Q. Li, and Q. Zhang, Opt. Lett. **34**, 2102 (2009).
[15] H. Du, H. Wang, and B. Hu, Phys. Rev. A **81**, 063813 (2010).
[16] T. Pfeifer, L. Gallmann, M. J. Abel, D. M. Neumark, and S. R. Leone, Opt. Lett. **31**, 975 (2006).
[17] F. Calegari, C. Vozzi, M. Negro, G. Sansone, F. Frassetto, L. Poletto, P. Villoresi, M. Nisoli, S. De Silvestri, and S. Stagira, Opt. Lett. **34**, 3125 (2009).
[18] Z. Zeng, Y. Cheng, X. Song, R. Li, and Z. Xu, Phys. Rev. Lett. **98**, 203901 (2007).

[19] C. Vozzi, F. Calegari, F. Frassetto, L. Poletto, G. Sansone, P. Villoresi, M. Nisoli, S. De Silvestri, and S. Stagira, Phys. Rev. A **79**, 033842 (2009).
[20] G. Orlando, P. P. Corso, E. Fiordilino, and F. Persico, J. Phys. B **43**, 025602 (2010).
[21] T. Pfeifer, L. Gallmann, M. J. Abel, P. M. Nagel, D. M. Neumark, and S. R. Leone, Phys. Rev. Lett. **97**, 163901 (2006).
[22] D. G. Lee, J. H. Kim, K. H. Hong, and C. H. Nam, Phys. Rev. Lett. **87**, 243902 (2001).
[23] J. J. Carrera, X. M. Tong, and S.-I. Chu, Phys. Rev. A **74**, 023404 (2006).
[24] J. J. Carrera and S.-I. Chu, Phys. Rev. A **75**, 033807 (2007).
[25] P. Zou, Z. Zeng, Y. Zheng, Y. Lu, P. Liu, R. Li, and Z. Xu, Phys. Rev. A **82**, 053411 (2010).
[26] M. Geissler, G. Tempea, A. Scrinzi, M. Schnürer, F. Krausz, and T. Brabec, Phys. Rev. Lett. **83**, 2930 (1999).
[27] M. B. Gaarde, J. L. Tate, and K. J. Schafer, J. Phys. B **41**, 132001 (2008).
[28] C. Altucci, V. Tosa, and R. Velotta, Phys. Rev. A **75**, 061401(R) (2007).
[29] C. Altucci, R. Esposito, V. Tosa, and R. Velotta, Opt. Lett. **33**, 2943 (2008).
[30] V. Tosa, K. Kovacs, C. Altucci, and R. Velotta, Opt. Express **17**, 17700 (2009).
[31] C. Altucci, R. Velotta, V. Tosa, P. Villoresi, F. Frassetto, L. Poletto, C. Vozzi, F. Calegari, M. Negro, S. De Silvestri, and S. Stagira, Opt. Lett. **35**, 2798 (2010).
[32] K. Schiessl, E. Persson, A. Scrinzi, and J. Burgdörfer, Phys. Rev. A **74**, 053412 (2006).
[33] M. Lewenstein, Ph. Balcou, M. Yu. Ivanov, A. L'Huillier, and P. B. Corkum, Phys. Rev. A **49**, 2117 (1994).
[34] M. V. Ammosov, N. B. Delone, and V. P. Krainov, Sov. Phys. JETP **64**, 1191 (1986).
[35] E. Priori, G. Cerullo, M. Nisoli, S. Stagira, S. De Silvestri, P. Villoresi, L. Poletto, P. Ceccherini, C. Altucci, R. Bruzzese, and C. de Lisio, Phys. Rev. A **61**, 063801 (2000).
[36] Z. Chang, Phys. Rev. A **70**, 043802 (2004).
[37] P. Lan, P. Lu, Q. Li, F. Li, W. Hong, and Q. Zhang, Phys. Rev. A **79**, 043413 (2009).
[38] P. Antoine, B. Piraux, and A. Maquet, Phys. Rev. A **51**, R1750 (1995).
[39] P. Antoine, A. L'Huillier, and M. Lewenstein, Phys. Rev. Lett. **77**, 1234 (1996).
[40] P. Salières, B. Carré, L. Le Déroff, F. Grasbon, G. G. Paulus, H. Walther, R. Kopold, W. Becker, D. B. Milosević, A. Sanpera, and M. Lewenstein, Science **202**, 902 (2001).